Acta Crystallographica Section D
Biological Crystallography
ISSN 0907-4449

Effect of mutations in the T1.5 loop of pectate lyase A from *Erwinia chrysanthemi* EC16

Seameen J. Dehdashti, Chuong N. Doan, Kinlin L. Chao† and Marilyn D. Yoder*

University of Missouri Kansas City, School of Biological Sciences, 5100 Rockhill Road, Kansas City, Missouri 64111-2499, USA

† Current address: CARB-UMBI, 9600 Gudelsky Drive, Rockville, MD 20850, USA.

Correspondence e-mail: yoderm@umkc.edu

Received 26 March 2003
Accepted 22 May 2003

PDB References: PelA T1.5 mutant, 2.9 Å, 1ooc, r1oocsf; PelA T1.5 mutant, 1.6 Å, 1pe9, r1pe9sf.

Pectate lyase A (PelA) is a pectate-degrading enzyme secreted by plant pathogens. PelA from *Erwinia chrysanthemi* has 61% amino-acid identity and a conserved structural similarity to pectate lyase E (PelE). Although similar in structure and sequence, the enzymatic characteristics of PelA differ from those for PelE. A structural alignment of PelA and PelE reveals differences in the T1.5 loop. The sequence of the T1.5 loop in PelA was mutated to the homologous sequence in PelE. The crystal structure of the PelA T1.5 mutant has been solved to 1.6 and 2.9 Å resolution. The enzymatic and structural properties of the T1.5 mutant are discussed.

1. Introduction

Erwinia chrysanthemi is a Gram-negative bacterium that causes soft-rot disease in plant tissues *via* the secretion of cell-wall-degrading enzymes. These enzymes are classified by substrate specificity and cleavage mechanism. One class of enzymes are pectate-degrading: this includes pectate lyases (Pel) and polygalacturonases (Collmer & Keen, 1986; Alfano & Collmer, 1996). They cleave the α-1,4-galacturonsyl linkages in pectate polymers that are structural components of the plant cell wall and middle lamella.

The Pel family in *E. chrysanthemi* consists of five major isozymes: PelA, PelB, PelC, PelD and PelE. Pels utilize a calcium-dependent β-elimination mechanism. The enzymatic properties of Pels differ in the length of their oligosaccharide endproducts, their plant-maceration activity and *in vitro* activity rates. The major Pel genes in *E. chrysanthemi* EC16 are organized as two multigene families on separate chromosomal clusters. The *pelA* and *pelE* genes reside in the same gene cluster and share 61% amino-acid identity (Tamaki *et al.*, 1988; Barras *et al.*, 1987). Although PelA and PelE share high amino-acid identity and conserved crystal structures, they differ significantly in their enzymatic properties (Payne *et al.*, 1987; Barras *et al.*, 1987; Beaulieu *et al.*, 1993).

The Pels have a parallel β-helix fold and the core of the protein consists of three parallel β-sheets: PB1, PB2 and PB3 (Fig. 1). These sheets are connected by loops, forming eight coils along an axis of constant diameter: T1 (connecting PB1 with PB2), T2 (between PB2 and PB3) and T3 (between PB3 and PB1). A single loop is designated by its position between the parallel β-sheets; for example, T1.5 refers to the T1 loop in the fifth coil on the parallel β-helix, counting from the N-terminus (Yoder *et al.*, 1993).

A structural comparison of PelE and PelA reveal two differences between the enzymes (Thomas *et al.*, 2002). The active-site groove of PelA is more negatively charged and that of PelE is more positively charged. Secondly, a structural difference in the T1.5 loop is observed, with the T1.5 loop in PelE exhibiting a different conformation from the PelA loop. Furthermore, the conformation of the T1.5 loop in both enzymes influences the orientation of an Arg side chain that has been shown to be significant in substrate cleavage (Scavetta *et al.*, 1999).

The crystal structure of the PelC substrate complex identified all residues involved in substrate binding (Scavetta *et al.*, 1999). A structural comparison of PelA, PelE and PelC revealed that the T1.5 loop affects the orientation of an arginine residue (Thomas *et al.*, 2002) which hydrogen bonds to the substrate near the putative scissile bond (Herron *et al.*, 2000). A PelA mutant was constructed in which four site-specific mutations changed the sequence of the T1.5 loop in PelA to the homologous sequence in PelE. The crystal structure of the PelA T1.5 mutant has been determined to 1.6 Å with synchrotron radiation and to 2.9 Å with Cu radiation.

2. Materials and methods

2.1. Construction of the T1.5 mutant

The T1.5 mutant of PelA was constructed from the pPEL812 plasmid (Keen & Tamaki, 1986). Four residues in the T1.5 loop region of PelA were mutated to match the structurally analogous T1.5 loop of PelE, using the QuickChange Site-Directed Mutagenesis Kit (Stratagene). These mutations using PelA

numbering are N215S, T217S, S219G and A220S. Sequencing was used to verify the T1.5 mutations in PelA. The plasmid construct containing the T1.5 mutant, pMDY29, was transformed into *Escherichia coli* DH5 α for protein expression.

2.2. Protein purification

Escherichia coli cells carrying the pMDY29 construct were grown in Luria–Bertani (LB) media containing 100 µg ml^{-1} ampicillin and induced at A_{600} = 1.0 with 0.6 m*M* isopropyl-β-D-thiogalactoside (IPTG). The periplasmic fraction containing the expressed protein was prepared by osmotic shock (Sambrook & Russell, 2001). Purification from the periplasmic fraction followed published procedures (Doan *et al.*, 2000).

Protein purity was assessed using SDS–PAGE (Laemmli, 1970) and matrix-assisted laser desorption ionization–time of flight (MALDI–TOF) mass spectrometry. Protein concentration was determined using an estimated extinction coefficient of 40 920 M^{-1} cm^{-1} based on the amino-acid sequence of the protein (Gill & von Hippel, 1989).

Enzymatic cleavage of the glycosidic bond was monitored by the increase in A_{232} arising from double-bond formation. The reaction mixture contained 50 m*M* 2-(*N*-cyclohexylamino)ethanesulfonic acid (CHES), 0.5 m*M* $CaCl_2$, 0.1%(*w*/*v*) sodium polygalacturonate (Sigma) and an appropriate amount of protein. One unit of Pel activity is defined as the production of 1 mmol of unsaturated product per minute. The formation of 1 mmol of unsaturated uronide per minute was taken to correspond to 1.73*A* units per minute (Zucker & Hankin, 1970).

2.3. Crystallization conditions

Crystals were grown at 295 K using hanging-drop vapor-diffusion techniques. The refined crystallization conditions consisted of a 0.8 ml reservoir solution consisting of 17.6–20% polyethylene glycol (PEG) 5000 monomethyl ether (MME) and 0.1 *M* 2-(*N*-morpholino)ethanesulfonic acid (MES) pH 6.5. The 0.006 ml drop contained 8.72 mg ml^{-1} of protein, 2.9–3.3% PEG 5000 MME and 0.02 *M* MES pH 6.5. Crystals typically appeared within 1–2 d.

2.4. Data collection and refinement

Using Cu radiation, X-ray data were collected on a MAR300 phospho-imaging-plate detector mounted on a Rigaku RU-200HB rotating-anode generator operating at 50 kV and 100 mA with Osmic blue confocal mirrors. The loop-mounted crystal was flash-cooled directly in the liquid-nitrogen stream. X-ray data were collected at 153 K with an exposure time of 240 s, an oscillation range of 1° and a crystal-to-detector distance of 250 mm.

Synchrotron data were collected at the Advanced Photon Source (APS) at Argonne National Laboratories on beamline 22ID. Single-wavelength X-ray data were collected at 1.000 Å on a MAR CCD165 detector with a crystal-to-detector distance of 180 mm. The oscillation range was 0.75° per frame, with an exposure time of 1 s. X-ray data were collected at 100 K from a crystal flash-cooled directly in the liquid-nitrogen stream.

X-ray diffraction images were indexed and scaled using *HKL* version 1.97.2 (Otwinowski & Minor, 1997). The crystal structure was initially solved and deposited in the PDB at 2.9 Å resolution. During manuscript review, a high-resolution 1.6 Å data set was collected and the structure was separately refined. Both crystal forms have $P2_12_12$ symmetry with similar unit-cell parameters. The structures were solved by molecular replacement as implemented in *AMoRe* (Navaza, 1994) within *CCP*4 version 4.2.1 (Collaborative Computational Project, Number 4, 1994). For each data set, 5% of the reflections were randomly selected for $R_{\rm free}$ statistics (Brünger, 1993).

CNS version 1.1 (Brünger *et al.*, 1998) was used for model refinement and electron-

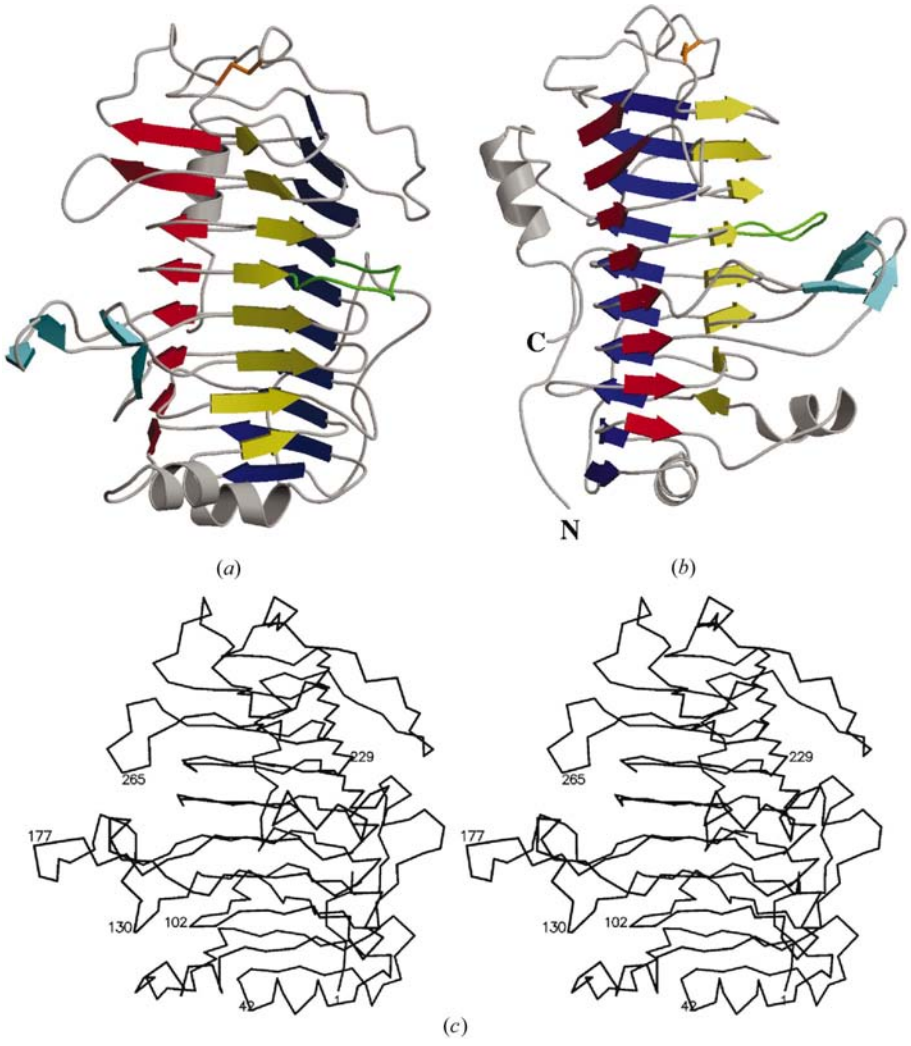

Figure 1
(*a*) A ribbon diagram of the PelA T1.5 mutant. The parallel β-sheets are shown in different colors: yellow for PB1, blue for PB2 and red for PB3. The two β-ribbons not participating in the parallel β-helix are shown in aqua. The disulfide bond is drawn as an orange thunderbolt and the T1.5 loop is shown in green. (*b*) A 90° rotation about the vertical axis of the orientation in (*a*). The N- and C-termini are labeled 'N' and 'C', respectively. (*c*) Stereo-image representation of the C^{α}-chain trace for the PelA T1.5 mutant. Residue numbers throughout the molecule are indicated. Figures were created using *MOLSCRIPT* version 2.1 (Kraulis, 1991) and rendered with *Raster3D* version 2.6 (Merritt & Bacon, 1997).

density map calculations. *O* version 7.0 was used for molecular graphics (Jones *et al.*, 1991). Solvent molecules were assigned using the *CNS* water-picking procedure. Peaks greater than 3σ were picked from an $F_{obs} - F_{calc}$ electron-density map using default distance criteria. All potential solvent molecules were checked in *O* (Jones *et al.*, 1991).

3. Results

3.1. T1.5 mutant characterization

The pH profiles of the T1.5 mutant, PelA and PelE demonstrated that the T1.5 mutant has the same pH profile as PelA. A comparison of the specific activities of the T1.5 mutant (1318 ± 41 U mg^{-1}), PelA (1015 ± 46 U mg^{-1}) and PelE (1291 ± 141 U mg^{-1}) at their respective optimal pHs revealed that the T1.5 mutant has a higher specific activity than PelA. A Student's *t*-test analysis on the specific activity of PelE and the T1.5 mutant concluded that there is no significant difference between the specific activity of these two enzymes.

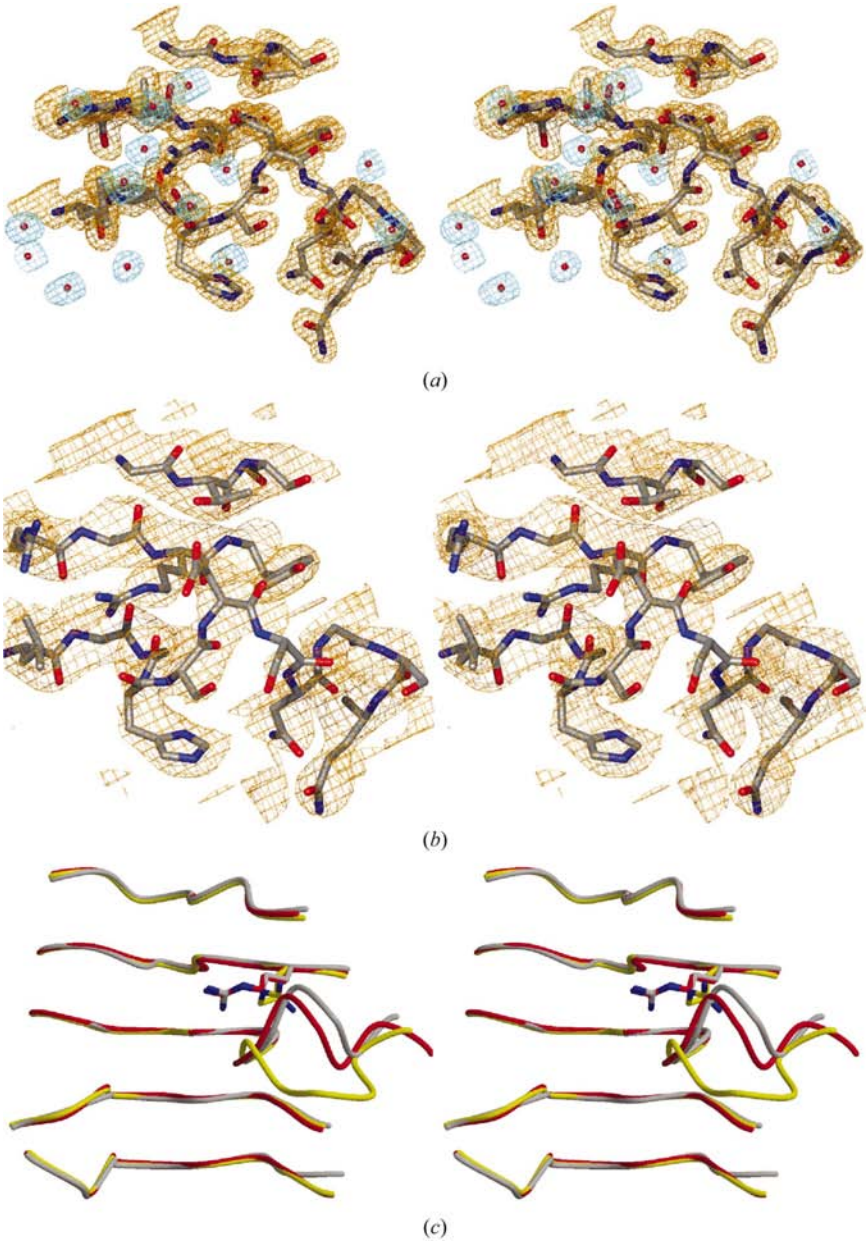

Figure 2
Stereo image of the electron-density map in the T1.5 loop region. Gold wire represents density for the protein and blue wire represents density for solvent molecules. Atom colors are shown in standard CPK coloring, with water molecules as red spheres. (*a*) The 1.6 Å model, (*b*) the 2.9 Å model and (*c*) stereo image of the superposition of the C$^{\alpha}$ trace of the active site and the T1.5 loop. The side-chain atoms of the Arg residue affected by the T1.5 loop are shown: Arg246 in PelA and the T1.5 mutant and Arg235 in PelE. PelA is depicted with a yellow trace and yellow C atoms, PelE is depicted with a gray trace and C atoms and the T1.5 mutant with a red trace and C atoms. Other atoms shown in standard CPK colors. Figs. 2(*a*) and 2(*b*) were created with *O* (Jones *et al.*, 1991) and rendered with *MOLRAY* version 1.3 (Harris & Jones, 2001). Fig. 2(*c*) was created using *MOLSCRIPT* version 2.1 (Kraulis, 1991) and rendered with *Raster3D* version 2.6 (Merritt & Bacon, 1997).

Table 1
Statistics for X-ray data collection using synchrotron and Cu radiation.

Values in parentheses indicate the highest resolution shell. The highest resolution range for the synchrotron data is 1.68–1.60 Å and that for the in-house data is 3.0–2.9 Å.

	Synchrotron	Cu $K\alpha$
Diffraction limit (Å)	1.6	2.9
Wavelength (Å)	1.000	1.542
Temperature (K)	100	153
Resolution (Å)	1.6	2.9
Reflections collected	564358	128721
Unique reflections	100459	14754
Completeness (%)	94.1 (71.2)	91.6 (81.0)
$\langle I/\sigma(I)\rangle$	29.61 (4.9)	23.6 (8.35)
$I > 3\sigma(I)$† (%)	87.1 (67.4)	84.1 (66.5)
R_{sym}‡ (%)	9.7 (20.2)	9.7 (27.3)
Mosaicity	0.212	0.80

† Percentage of data with $I > 3\sigma(I)$. ‡ $R_{sym} = \sum(I_{hkl} - \langle I_{hkl}\rangle)/\sum I_{hkl}$ (single measurements excluded).

Table 2
Refinement and model statistics for both models.

	Synchrotron	Cu $K\alpha$
Resolution range (Å)	50.0–1.6	50.0–2.9
No. of reflections (No. in test set)	94503 (5020)	14701 (1511)
R_{cryst}† (R_{free}) (%)	19.79 (21.32)	21.95 (27.48)
No. of atoms		
Protein	5450	5458
Water molecules	780	0
R.m.s.d. *B* factors (Å^2)		
Main-chain bonds	1.024	0.956
Main-chain angles	1.558	1.610
Side-chain bonds	1.927	1.377
Side-chain angles	2.707	2.112
Average *B* values (Å^2)		
Protein main chain	14.174	16.373
Protein side chain	18.461	16.539
Water molecules	25.450	0
R.m.s.d. from ideality		
Bond length (Å)	0.005	0.008
Bond angle (°)	1.40	1.57
Dihedrals (°)	26.5	25.665
Ramachandran plot‡		
Favored (%)	86.0	76.1
Allowed (%)	13.5	21.5
Generously allowed (%)	0.2	2.1
Disallowed (%)	0.3	0.3

† $R_{cryst} = \sum[F(obs)_{hkl} - F(calc)_{hkl}]/\sum F(obs)_{hkl}$. ‡ Glycines and prolines excluded from calculations.

3.2. Structure of the T1.5 mutant

Statistics for both X-ray data sets are shown in Table 1. The crystal structure of the T1.5 mutant has been solved at 1.6 and 2.9 Å resolution using synchrotron and Cu radiation, respectively. PelA (PDB code 1jta) was used as the molecular search model for both

crystal structures, in which residues 213–225 (the T1.5 loop) and the side-chain atoms of residue Arg246 were computationally removed. The missing residues in the T1.5 loop region were manually built into electron-density maps. The refined model for both data sets consists of two molecules in the asymmetric unit with all residues in the protein (1–361).

The structure was initially solved to 2. 9 Å resolution; during manuscript review the 1.6 Å data was collected and the structure was refined. The 1.6 Å model consists of 780 water molecules (Table 2). No water molecules were built for the 2.9 Å model owing to resolution limits. Non-crystallographic symmetry (NCS) restraints of 300 were used in the refinement process for both data sets and were gradually relaxed to 50 for the 2.9 Å data and completely released for the 1.6 Å data, using $R_{\rm free}$ statistics as a guide. One residue, Tyr247, has an unfavorable combination of ψ, φ backbone torsion angles in both data sets, as determined by *PROCHECK* (Laskowski *et al.*, 1992). The same residue has unfavorable backbone torsion angles in the 1.9 Å resolution crystal structure of native PelA (Thomas *et al.*, 2002).

3.3. The T1.5 loop of PelA, PelE and the T1.5 loop

A structural analysis of PelA, PelE and PelC revealed differences in the conformation of the T1.5 loop which affected the orientation of an Arg residue (Thomas *et al.*, 2002). In PelA, the T1.5 loop has a random-coil structure, removing a steric constraint and allowing the Arg246 side chain, unlike in PelE and PelC, to be orientated away from the active-site groove (Thomas *et al.*, 2002). The final electron-density map in the T1.5 loop region is shown in Fig. 2. A superposition of the T1.5 loop regions of PelA, the T1.5 mutant and PelE reveals that the T1.5 loop in the PelA mutant has changed to an α-helical conformation, similar to that in PelE (Fig. 2). Furthermore, the Arg246 side chain in the T1.5 mutant is oriented into the active-site groove.

4. Conclusions

The T1.5 mutant was constructed to gain insight into the properties that determine the enzymatic differences between PelA and PelE. The two enzymes have 61% amino-acid identity with highly conserved superposition of the C^{α} atoms. A structural difference between PelA and PelE was observed in the T1.5 loop. In PelA the loop has a random-coil structure, whereas in PelE and PelC the loop has a short α-helical element (Thomas *et al.*, 2002). The side-chain atoms of Arg246 of PelA are orientated away from the active-site groove, whereas the side-chain atoms in the analogous residue of PelE, Arg235, are oriented towards the active-site groove.

The results of enzymatic assays on the T1.5 mutant revealed that the pH optimum of the T1.5 mutant is identical to that of PelA, but the T1.5 mutant has an increased specific activity that is comparable to that of PelE.

The crystal structure of the T1.5 mutant was solved to 1.6 and 2.9 Å resolution. Both structures revealed a conformation change in the T1.5 loop from the PelA conformation to that observed in PelE (Fig. 2). Furthermore, the conformation of the T1.5 loop has restricted the side chain of Arg246 into the active-site groove of the mutant.

MALDI–TOF mass spectrometry was performed by UMKC mass spectrometry facility under the supervision of Dr Antonio Artiques. Structural coordinates of PelE were a courtesy of Frances Jurnak, University of California, Riverside. Use of the Advanced Photon Source was supported by the US Department of Energy, Office of Science, Office of Basic Energy Sciences under Contract No. W-31-109-Eng-38. Data were collected at the Southeast Regional Collaborative Access Team (SER-CAT) 22-ID beamline at the Advanced Photon Source, Argonne National Laboratory. Supporting institutions may be found at http://www.ser.anl.gov/new/index.html. This work was supported by a grant from the National Science Foundation (MDY).

References

Alfano, J. R. & Collmer, A. (1996). *Plant Cell*, **8**, 1683–1698.
Barras, F., Thurn, K. K. & Chatterjee, A. K. (1987). *Mol. Gen. Genet.* **209**, 319–325.
Beaulieu, C., Boccara, M. & Gijsegem, F. V. (1993). *Mol. Plant Microb. Interact.* **6**, 197–202.
Brünger, A. T. (1993). *Acta Cryst.* D**49**, 24–36.
Brünger, A. T., Adams, P. D., Clore, G. M., Gros, P., Grosse-Kunstleve, R. W., Jiang, J.-S., Kuszewski, J., Nilges, M., Pannu, N. S., Read, R. J., Rice, L. M., Simonson, T. & Warren, G. L. (1998). *Acta Cryst.* D**54**, 905–921.
Collaborative Computational Project, Number 4 (1994). *Acta Cryst.* D**50**, 760–763.
Collmer, A. & Keen, N. T. (1986). *Annu. Rev. Phytopathol.* **24**, 383–409.
Doan, C. N., Caughron, M. K., Myers, J. C., Breakfield, N. W., Oliver, R. L. & Yoder, M. D. (2000). *Acta Cryst.* D**56**, 351–353.
Gill, S. C. & von Hippel, P. H. (1989). *Anal. Biochem.* **182**, 319–326.
Harris, M. & Jones, T. A. (2001). *Acta Cryst.* D**57**, 1201–1203.
Herron, S. R., Benen, J. A., Scavetta, R. D., Visser, J. & Jurnak, F. (2000). *Proc. Natl Acad. Sci.* **97**, 8762–8769.
Jones, T. A., Cowan, S., Zou, J.-Y. & Kjeldgaard, M. (1991). *Acta Cryst.* A**47**, 110–119.
Keen, N. T. & Tamaki, S. (1986). *J. Bacteriol.* **168**, 595–606.
Kraulis, P. J. (1991). *J. Appl. Cryst.* **24**, 946–950.
Laemmli, U. K. (1970). *Nature (London)*, **227**, 680–685.
Laskowski, R. A., MacArthur, M. W., Moss, D. S. & Thornton, J. M. (1992). *J. Appl. Cryst.* **26**, 283–291.
Merritt, E. A. & Bacon, D. J. (1997). *Methods Enzymol.* **277**, 505–524.
Navaza, J. (1994). *Acta Cryst.* A**50**, 157–163.
Otwinowski, Z. & Minor, W. (1997). *Methods Enzymol.* **276**, 307–326.
Payne, J. H., Schoedel, C., Keen, N. T. & Collmer, A. (1987). *Appl. Environ. Microbiol.* **53**, 2315–2320.
Sambrook, J. & Russell, D. W. (2001). *Molecular Cloning*. New York: Cold Spring Harbor Laboratory Press.
Scavetta, R. D., Herron, S. R., Hotchkiss, A. T., Kita, N., Keen, N. T., Benen, J. A., Kester, H. C., Visser, J. & Jurnak, F. (1999). *Plant Cell*, **11**, 1081–1092.
Tamaki, S. J., Gold, S., Robeson, M., Manulis, S. & Keen, N. T. (1988). *J. Bacteriol.* **170**, 3468–3478.
Thomas, L. M., Doan, C. N., Oliver, R. L. & Yoder, M. D. (2002). *Acta Cryst.* D**58**, 1008–1015.
Yoder, M. D., Lietzke, S. & Jurnak, F. (1993). *Structure*, **1**, 241–251.
Zucker, M. & Hankin, L. (1970). *J. Bacteriol.* **104**, 13–18.